Optical properties and microstructure of Ta_2O_5 thin films prepared by oblique angle deposition

Xiudi Xiao (肖秀娣)[1,2*], Guoping Dong (董国平)[1,2], Hongbo He (贺洪波)[1], Hongji Qi (齐红基)[1,3], Zhengxiu Fan (范正修)[1], and Jianda Shao (邵建达)[1]**

[1]*Shanghai Institute of Optics and Fine Mechanics, Chinese Academy of Sciences, Shanghai 201800, China*

[2]*Graduate University of Chinese Academy of Sciences, Beijing 100049, China*

[3]*Shanghai Daheng Optics and Fine Mechanics Co., Ltd., Shanghai 201800, China*

[*]*E-mail: piaopiao1008@163.com;* [**]*e-mail: jdshao@mail.shcnc.ac.cn*

Received December 22, 2008

Tantalum pentoxide thin films are prepared by oblique angle electron beam evaporation. The influence of flux angle on the surface morphology and microstructure is investigated by scanning electron microscopy (SEM). The Ta_2O_5 thin films are anisotropic with highly orientated nanostructure of slanted columns. The porous microstructure of the as-deposited films results in the decrease of effective refractive index and packing density with increasing deposition angle. The anisotropic structure results in optical birefringence. The in-plane birefringence increases with the increase of deposition angle and reaches the maximum of 0.055 at the deposition angle of 70°. Anisotropic microstructure and critical packing density are the two key factors to influence the in-plane birefringence.

OCIS codes: 310.0310, 240.0240.

doi: 10.3788/COL20090710.0967.

Recently, oblique angle deposition (OAD) technique has attracted great attention due to its flexibility and low cost in the fabrication of variable nanostructures. Through tuning the obliquity and rotation speed of the substrate, a variety of nanostructures such as pillar, helix, zigzag, chevron, and dendritic shape can be fabricated[1]. Due to the characteristic microstructure, films prepared by OAD can be extensively used in optics[2−4], chemistry[5], biology[6], and medicine[7] fields.

Tantalum pentoxide (Ta_2O_5) is an important material and is widely used in industrial applications such as low-inductance decoupling capacitors[8], alternative gate insulator in field effect transistors[9,10], heat-barrier coatings[11], etc. It also has high refractive index, large band gap, excellent chemical stability, almost free-absorption at 300−2000 nm[12], making it an important potential material in optical applications such as filters, solar cells, charge-coupled devices (CCDs), and high power laser equipments[13−15].

In this letter, we prepare Ta_2O_5 thin films with OAD technique. The tilted nanocolumn microstructure is obtained through tuning the oblique angle of the substrate. Through scanning electron microscopy (SEM), ultraviolet/visible/near infrared (UV-vis-NIR) spectra and optical anisotropy measurements, the relationship between the microstructure and optical properties of the films is investigated.

Ta_2O_5 thin films were prepared by oblique angle electron beam (EB) evaporation at a base pressure of 2.0×10^{-3} Pa. BK7 glasses ($\Phi30\times3$ (mm)) and n-Si (100) substrates were ultrasonically cleaned in acetone and ethanol before introducing into the vacuum system. Granular Ta_2O_5 (purity 99.99%) were evaporated from an EB source located 27 cm from the substrate at an O_2 pressure of 2.7×10^{-2} Pa with a deposition rate of 0.76 nm/s. The deposition equipment was similar to that in our previous work[16]. The substrate tilted angle α was measured as the direction of the incident flux with respect to the substrate normal. In our experiment, the deposition angle α was fixed to be 0°, 40°, 60°, 70°, and 80° without substrate rotation. During deposition, the substrate was kept at room temperature. The nominal film thickness of 1.7 μm was controlled by the optical thickness monitor.

The composition of the thin films was measured by energy dispersive spectroscopy (EDS) equipped on SEM (JSM-6535). Before EDS measurements, the sample was deposited by a layer of carbon about several nanometers for conduction. The morphology was observed by field emission scanning electron microscopy (FE-SEM) in HITACHI S-4700 microscope. For SEM observation, Ta_2O_5 films were coated with a thin layer of gold to improve conduction. The cross-section was cleaved along the deposition plane. The UV-vis-NIR spectra of the films were measured by a Lambda 900 spectrophotometer. For the polarization measurement, a polarizer was introduced into the light path. The incident lights were two orthogonal polarization lights normal to the substrate surface. The light incident plane was parallel to the deposition plane and the wavelength range was 400−800 nm.

Figure 1 shows the composition of as-deposited thin films by EDS. It can be found that there is no other impurity in the thin films except for Ta and O elements. According to the analysis of element contents, the contents of Ta_2O_5 is about 95.89 wt.-% and C is about 4.11 wt.-%, which means that as-deposited thin film is stoichiometry. Hence the as-deposited thin films are Ta_2O_5 thin films.

Figure 2 shows the SEM images of Ta_2O_5thin films deposited at different oblique angles. Through the top-view images, it is found that films are loose and porous. Size and number of the pores increase with the increase of oblique angle. At the deposition angle $\alpha = 40°$, the film surface is smooth and no distinct pores can be ob-

 © 2009 Chinese Optics Letters

served. At $\alpha = 60°$, the film surface is rough with many apparent pores. While at $\alpha = 80°$, the film surface is full of nanoclusters and pores. The nanoclusters are irregular with many small nanocolumns inside. Through the cross-sectional images, it is observed that films consist of tilted nanocolumns and open pores, which is consistent with the results in Ref. [17]. The columns incline towards one direction (flux direction) due to oblique deposition and shadowing effects[18]. These cross-sectional morphologies are in agreement with the zone I structure of Thornton's model[19], which is caused by the limited mobility of the incoming atoms during oblique deposition. As the flux incident angle changes from 40° to 80°, the intercolumnar spacing and obliquity of columns increase with the increase of flux angle. The highly orientated nanostructure of the slanted columns indicates that Ta_2O_5 thin films are anisotropy with the long axis parallel to the columnar growth direction. The anisotropic structure will induce the anisotropic dependence on the thermal, electrical, magnetic, and optical properties of thin films[20]. Compared with the top-view and cross-sectional images at $\alpha = 80°$, the fan-out effect is obvious. At the beginning, nanocolumns grow separately and the columnar diameter is homogeneous. As the growth continues, some small columns stop growth and others cluster together to form larger columns, leading to the structural hierarchy shown in Fig. 2.

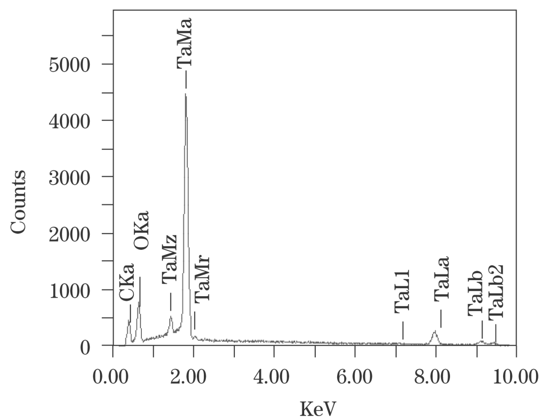

Fig. 1. Composition of as-deposited Ta_2O_5 thin films by EDS.

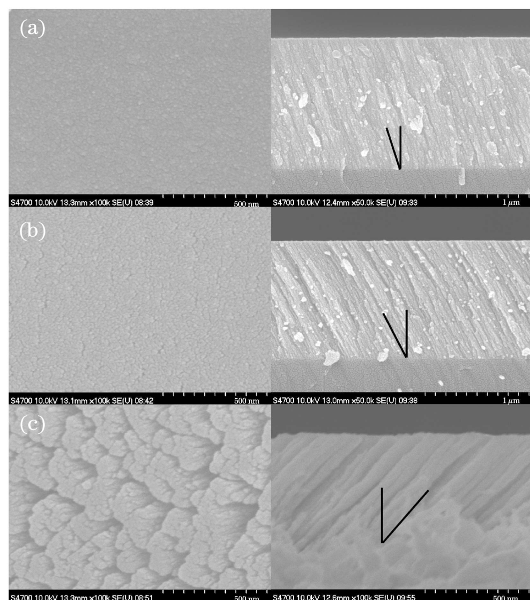

Fig. 2. Top-view (left) and corresponding cross-sectional (right) images of Ta_2O_5 thin films deposited at (a) 40°, (b) 60°, and (c) 80°, respectively.

The column angle β, defined as the angle between the substrate normal and the long axis of slanted columns, is a significant structural parameter with optical properties. The experimental and estimated column angle β are illustrated in Fig. 3. It can be seen that the column angle β is less than the deposition angle α. Besides, the column angle β increases with the increase of deposition angle α. An empirical formula known as tangent rule ($\tan\beta = 0.5\tan\alpha$) was proposed to estimate the function of α and β[21]. The experimental column angle measured from SEM images is about 18° at $\alpha = 40°$, which is close to the value estimated by tangent rule. However, the difference between the experimental and estimated values grow larger for $\alpha > 60°$, as shown in Fig. 3. Another formula known as cosine rule ($2\sin(\alpha-\beta) = 1-\cos\alpha$) can be much more successful in estimating the column angle of thin films deposited at larger deposition angles ($\alpha > 60°$)[22]. It can be found that the measured column angle deviates from the empirical formula, which might be due to the sensitivity of the columnar structure on deposition and material dependent parameters. Additionally, the great surface curvature of nanostructure films grown by OAD

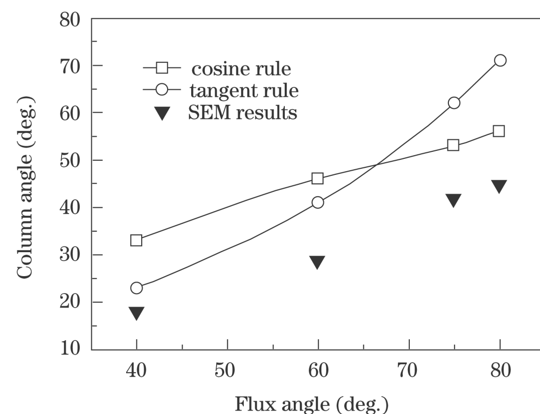

Fig. 3. Column angle versus flux incident angle α.

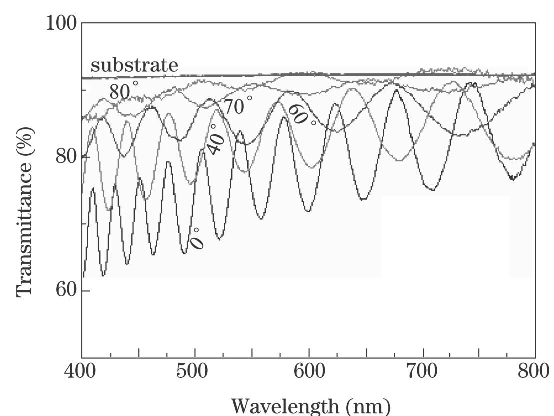

Fig. 4. Transmission spectra of Ta_2O_5 thin films deposited at 0°, 40°, 60°, 70°, and 80°, respectively.

will distinctly change the direction of column growth and can also induce the deviation.

The UV-vis-NIR transmittance spectra of thin films deposited at different angles are shown in Fig. 4. For the films with given thickness, due to the interference of the incident light, constructive wave interference and destructive wave interference occur periodically. Hence, the transmittance spectra of Ta_2O_5 films exhibit many peaks and valleys. However, due to the absorption and diffuse scattering of porous thin films, the maximum and minimum of transmittance spectra deviate from those of the substrate because of the refractive indices of thin films higher and smaller than substrate, respectively. It can be still found that the maximum of transmittance increases with the increase of incident angle. It is known that Ta_2O_5 is a high refractive index material ($n = 2.2$ at $\lambda = 550$ nm). The single-layer Ta_2O_5 on BK7 glass substrate is a reflectance film and the maximum transmission is lower than that of the substrate. While for $\alpha = 80°$, the transmission is slightly higher than that of the substrate, which means that n is close to the refractive index of the substrate. If thin films are deposited at higher incident angle, n can be smaller than the refractive index of the substrate and single-layer Ta_2O_5 can be used as anti-reflective films.

According to the transmission spectra, the optical constants of thin films at different angles are calculated by the envelope method[23]. The dispersion curves at wavelengths of 400−700 nm are fitted by Cauchy dispersion equation ($n(\lambda) = P_1 + P_2/\lambda^2 + P_3/\lambda^4$, $k(\lambda) = A_1 + A_2/\lambda^2 + A_3/\lambda^4$, where P_1, P_2, P_3, A_1, A_2, and A_3 are all the fitting parameters), as shown in Fig. 5. It is found that the refractive index n and extinction coefficient k decrease with the increase of incident angle α. With the incident angle increasing, the columnar spacing is increasing and columns are more apart. There are more pores in the films. Hence, the effective refractive index inevitably decreases. While due to the increasing columnar spacing, the oxidation is more efficient and adequate. Therefore, the absorption and k are also decreasing. Based on the Burggeman effective-medium approximation[24],

$$p_{\rm A}\frac{\varepsilon_{\rm A}-\varepsilon}{\varepsilon_{\rm A}+2\varepsilon}+p_{\rm B}\frac{\varepsilon_{\rm B}-\varepsilon}{\varepsilon_{\rm B}+2\varepsilon}=0, \quad (1)$$

where ε, ε_A, and ε_B are the dielectric functions of effective medium, material A, and material B; p_A and p_B represent the packing densities of materials A and B, respectively. The relationship between refractive index n at $\lambda = 550$ nm and the corresponding packing density p can be obtained, as shown in Fig. 6. It can be found that n and p are decreasing with the increase of incident angle. When the incident atoms arrive at the substrate surface normally, Ta_2O_5 films are compact and the packing density is close to 1. At $\alpha = 0°$, n is about 2.11 and p is about 98% of the bulk. While for $\alpha = 80°$, n is about 1.56 and p is only about 52% of the bulk. The decrease of refractive index and packing density in OAD Ta_2O_5 film can be ascribed to the porous structure in SEM images. By adjusting the flux incident angle, the effective index and packing density of OAD films can be engineered in a continuous range of values. One can also combine the microstructure evolution with the tailorable refractive index to produce refractive index gradient materials and other new optical filters.

When the transmission spectra are measured with two orthogonal polarized lights, in-plane birefringence is defined as the difference (Δn) of two in-plane refractive indices[25]. Figure 7 illustrates the in-plane birefringence Δn of Ta_2O_5 OAD films. The birefringence increases with the flux incident angle. At $\alpha = 70°$, the birefringence reaches the maximum of 0.055. A greater flux incident angle results in a decrease of birefringence, which means that there is an optimum deposition angle for the maximal birefringence. Small incident angle results in weakly anisotropic structure, while too large incident angle induces too much porous structure, which does not favor the improvement of in-plane birefringence. Anisotropic microstructure and packing density can be balanced with each other. There is a critical packing density to determine the in-plane birefringence[26]. According to the results shown in Fig. 6, it can be deduced that the critical packing density for Ta_2O_5 is about 0.56, which is consistent with the result calculated by effective medium model. The maximum birefringence of OAD Ta_2O_5 films is higher than that of some common crystals (e.g., for MgF_2, $\Delta n = 0.012$; for quartz, $\Delta n = 0.009$). It is suggested that OAD can offer an effective method to obtain the larger birefringence and it is flexible to design wave plate and polarizer.

In conclusion, Ta_2O_5 thin films prepared by OAD technique are anisotropic with highly orientated slanted columns. The column angle of thin films is smaller than the incident angle and increases with the increase of flux incident angle. Due to the shadowing effect and low atom mobility, the Ta_2O_5 thin films are a mixture of tilted columns and pores. The porous microstructure of the as-deposited films results in the decrease of effective refractive index and packing density with increasing

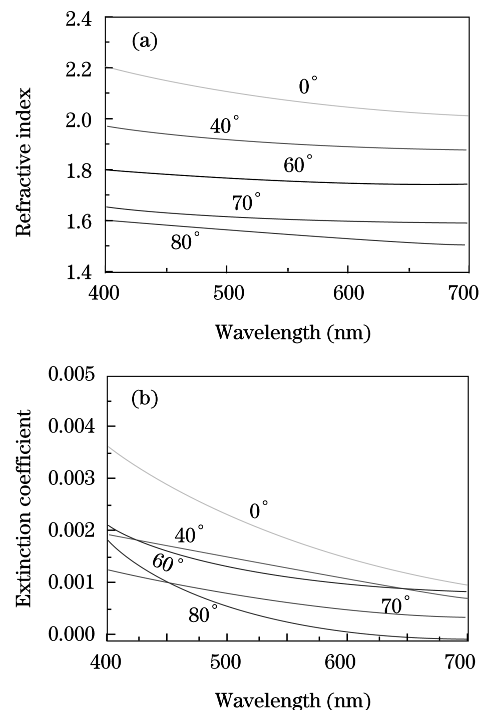

Fig. 5. Dispersion curves of optical constants. (a) Refractive index; (b) extinction coefficient.

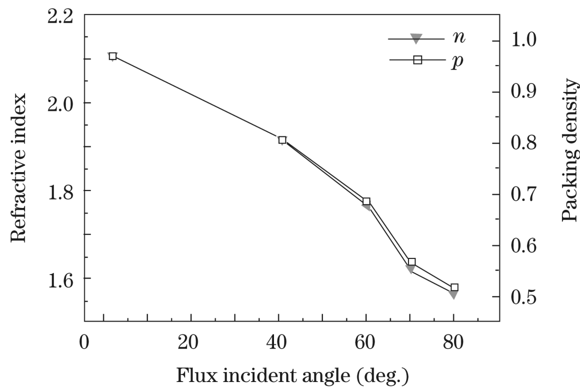

Fig. 6. Refractive index and packing density versus flux incident angle α at $\lambda = 550$ nm.

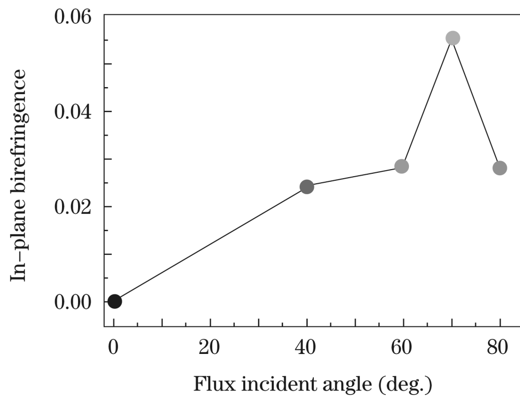

Fig. 7. In-plane birefringence versus flux incident angle α.

deposition angle. The anisotropic microstructure results in the optical anisotropy and forms the birefringence which varies as a function of the flux angle and reaches the maximum of 0.055 at $\alpha = 70°$. The OAD technique is an effective method to obtain large birefringence. Ta_2O_5 thin film deposited by OAD is a potential candidate for phase retarder and polarizer.

This work was supported by the National Natural Science Foundation of China (No. 60778026) and the Shanghai Rising-Star Program (No. 07QB14006).

References

1. K. Robbie, G. Beydaghyan, T. Brown, C. Dean, J. Adams, and C. Buzea, Rev. Sci. Instrum. **75,** 1089 (2004).
2. J.-Q. Xi, M. F. Schubert, J. K. Kim, E. F. Schubert, M. Chen, S.-Y. Lin, W. Liu, and J. A. Smart, Nature Photon. **1,** 176 (2007).
3. A. C. van Popta, M. H. Hawkeye, J. C. Sit, and M. J. Brett, Opt. Lett. **29,** 2545 (2004).
4. K. Kaminska, T. Brown, G. Beydaghyan, and K. Robbie, Appl. Opt. **42,** 4212 (2003).
5. Q. Zhou, Z. Li, Y. Yang, and Z. Zhang, J. Phys. D **41,** 152007 (2008).
6. R. A. Tripp, R. A. Dluhy, and Y. Zhao, Nanotoday **3,** (3-4) 31 (2008).
7. A. K. Kalkan, M. R. Henry, H. Li, J. D. Cuiffi, D. J. Hayes, C. Palmer, and S. J. Fonash, Nanotechnol. **16,** 1383 (2005).
8. H. Kimura, J. Mizuki, S. Kamiyama, and H. Suzuki, Appl. Phys. Lett. **66,** 2209 (1995).
9. E. Atanassova, N. Stojadinovic, A. Paskaleva, D. Spassov, L. Vracar, and M. Georgieva, Semicond. Sci. Technol. **23,** 075017 (2008).
10. M. Matsui, H. Nagayoshi, G. Muto, S. Tanimoto, K. Kuroiwa, and J. Tarui, Jpn. J. Appl. Phys. **29,** 62 (1990).
11. P. Kofstad, J. Electrochem. Soc. **109,** 776 (1962).
12. J. D. T. Kruschwitz and W. T. Pawlewicz, Appl. Opt. **36,** 2157 (1997).
13. F. Rubio, J. Denis, J. M. Albella, and J. M. Martinez-Duart, Thin Solid Films **90,** 405 (1982).
14. C. Xu, H. Dong, Q. Xiao, J. Ma, Y. Jin, and J. Shao, Chinese J. Lasers (in Chinese) **35,** 1595 (2008).
15. X. He, J. Wu, L. Zhao, J. Meng, X. Gao, and X. Li, Solid State Commun. **147,** 90 (2008).
16. S. Wang, X. Fu, G. Xia, J. Wang, J. Shao, and Z. Fan, Appl. Surf. Sci. **252,** 8734 (2006).
17. J. Ni, Y. Zhu, Q. Zhou, and Z. Zhang, J. Am. Ceram. Soc. **91,** 3458 (2008).
18. R. Messier, V. C. Venugopal, and P. D. Sunal, J. Vac. Sci. Technol. A **18,** 1538 (2000).
19. J. A. Thornton, Annu. Rev. Mater. Sci. **7,** 239 (1977).
20. B. Dick and M. J. Brett, in *Encyclopedia of Nanoscience and Nanotechnology.* vol. 6 (American Scientific Publishers, Valencia, 2004) pp. 703-725.
21. J. M. Nieuwenhuizen and H. B. Haanstra, Philips Tech. Rev. **27,** 87 (1966).
22. R. N. Tait, T. Smy, and M. J. Brett, Thin Solid Films **226,** 196 (1993).
23. Y. Wang, W. Zhang, Z. Fan, J. Huang, Y. Jin, J. Yao, and J. Shao, Chinese J. Lasers (in Chinese) **35,** 760 (2008).
24. V. Janicki, J. Sancho-Parramon, and H. Zorc, Thin Solid Films **516,** 3368 (2008).
25. G. Beydaghyan, K. Kaminska, T. Brown, and K. Robbie, Appl. Opt. **43,** 5343 (2004).
26. J. Wang, J. Shao, and Z. Fan, Opt. Commun. **247,** 107 (2005).